Physica B 680 (2024) 415836

Contents lists available at ScienceDirect

Physica B: Condensed Matter

journal homepage: www.elsevier.com/locate/physb

# Thermoluminescence (TL) and electron paramagnetic resonance (EPR) of dumortierite sensitized by heat treatments

Betzabel N. Silva-Carrera [a], T.K. Gundu Rao [b], Betzabeth J. Lopez-Flores [b], Jorge S. Ayala-Arenas [b], René R. Rocca [c], J.F. Benavente [d], Jose F.D. Chubaci [e], Nilo F. Cano [b,c,*]

[a] Instituto de Pesquisas Energéticas e Nucleares, IPEN-CNEN/SP, São Paulo, SP, Brazil
[b] Universidad Nacional de San Agustín de Arequipa - UNSA, Peru
[c] Universidade Federal de São Paulo, Instituto do Mar, Santos, SP, Brazil
[d] CIEMAT, Av. Complutense 40 E, 28040, Madrid, Spain
[e] Universidade de São Paulo, Instituto de Física, São Paulo, SP, Brazil

ARTICLE INFO

*Keywords:*
Dumortierite
Defect centers
TL
EPR

ABSTRACT

The present study presents the effect of heat treatment on TL and EPR of dumortierite. It was found that applying a heat treatment at 1200 °C for 1h, followed by slow cooling to room temperature, is optimal for improving its TL sensitivity. The glow curves of the sensitized dumortierite sample show TL emission bands centered at 350, 475, and 580 nm. The kinetic parameters of the TL peaks were obtained using the Tm-Tstop and deconvolution methods. In addition, sensitized dumortierite exhibits a linear response with γ-radiation dose and low fading in its TL response. Studies using the technique of EPR were carried out to investigate the defect center EPR signals observed after γ-irradiation. A single defect center with an axially symmetric *g*-tensor was observed with principal values $g_{\parallel} = 2.0009$ and $g_{\perp} = 2.0017$. The center was attributed to an $F^{+}$ center and appears to correlate with the TL peak at 200 °C.

## 1. Introduction

Thermoluminescence (TL) arises from the presence of intrinsic and extrinsic point defects within the crystal lattice matrix and Electron Paramagnetic Resonance (EPR) is observable from such defects if they are paramagnetic with unpaired electrons [1–3]. Therefore, it is important to explore and elucidate the correlation between TL and EPR, in the specific case of dumortierite, the mineral studied in the present investigation. The dumortierite crystal group is divided into three groups: (1) dumortierite (Al, ⊡)$Al_6BSi_3O_{16}(O,OH)_2$; (2) magnesiodumortierite (Mg, ⊡)$Al_6BSi_3O_{16}(O,OH)_2$; (3) and holtite (Al,Ta, ⊡)$Al_6B$(Si, Sb, As)$_3O_{15}$(O,OH, ⊡)$_1$, where ⊡ represents a cation or anion vacancy [4].

Dumortierite is an aluminum borosilicate, being the second most abundant borosilicate after tourmaline [5]. This crystal can form as pegmatites, aplites, and in medium-to high-grade metamorphic rocks and can be of regional or contact type [6]. There is dumortierite of different colors, and it presents pleochroism, observing colors such as blue, violet, lilac, red, yellow, and brown [7]. Intense blue dumortierite occurs in Veheragala, north of Habarana, Sri Lanka, and there are more than 40 localities worldwide where dumortierite occurs [8].

The chemical analysis of some dumortierite samples shows the presence of compounds in higher concentrations, such as $P_2O_5$, MgO, $TiO_2$, $Fe_2O_3$, FeO, $H_2O$, $B_2O_3$ [9], $Al_2O_3$, and $SiO_2$. On the other hand, other works showed the presence of $As_2O_3$, $Sb_2O_3$, $Ta_2O_5$, and $Nb_2O_5$ in significant amounts, and a few samples of this crystal contain $Bi^{3+}$ [4].

Horn et al. [5] studied dumortierites from different regions of Brazil (Minas Gerais and Bahia) and other countries such as Canada, United States, Chile, and Madagascar, using the techniques of EPR, infrared (IR) spectroscopy, and Mössbauer spectroscopy.

According to Meshram and Ingle [10], the main minerals associated with natural dumortierite are muscovite, kyanite, pyrophyllite, and corundum, while dravite, gobbinisite, diaspore, and microcline are present in smaller proportions. The dumortierite also presents pleochroism from colorless to light pink and from light blue to violet in the form of needles or fibrous crystals. Choo and Kim [11] used X-ray diffraction (XRD) and electron microprobe analyzer (EPMA) techniques to identify the crystalline phases and chemical composition, respectively, of Korean clay samples, showing that dumortierite is formed at an early stage upon hydrothermal alteration, and then pyrophyllite is

* Corresponding author. Universidade Federal de São Paulo, Instituto do Mar, Santos, SP, Brazil.
*E-mail addresses:* nilocano@if.usp.br, nilo.cano@unifesp.br (N.F. Cano).

https://doi.org/10.1016/j.physb.2024.415836
Received 20 January 2024; Received in revised form 17 February 2024; Accepted 5 March 2024
Available online 8 March 2024

formed by the addition of silicon to its structure. Werding and Schreyer [6] synthesized dumortierite using $Al_2O_3$, $B_2O_3$, $SiO_2$, $H_2O$, and $H_3BO_3$ for different pressure and temperature conditions. In all the synthesized samples, they found the presence of quartz attached to the dumortierite.

Studies on other minerals show that heat treatment and γ-irradiation can affect some physical properties, such as TL and EPR. On this background, in the present work, we have studied the effect of heat treatment and γ-irradiation on the thermoluminescence (TL) and electron paramagnetic resonance (EPR) properties associated with the luminescent and paramagnetic centers of natural dumortierite from Peru.

## 2. Material and methods

The dumortierite studied in this work comes from the city of Canta, Lima, Peru. This dumortierite sample was crushed and carefully ground using an agate mortar and pestle, then sieved to retain grains with a diameter between 0.080 and 0.180 mm for TL and EPR measurements. Samples with grains smaller than 0.080 mm in diameter were used for X-ray diffraction (XRD) and X-ray fluorescence (XRF) measurements. The chemical analysis of the natural dumorteirite was carried out using PANalytical XRF equipment, model Zatium. The study of the crystalline structure of the material was performed by powder XRD using a Rigaku diffractometer, model Miniflex 600, with $CuK_\alpha$ radiation (40 kV, 1.5 mA). TL measurements were performed with the Harshaw model 4500 TL reader in a nitrogen atmosphere with a heating rate of 4 °C/s. TL light was detected using a Hamamatsu R647 photomultiplier tube and a Schott KG1 filter with a transmission band between 330 and 690 nm. Five TL reading measurements were carried out to obtain an average TL glow curve. A mass of 4.0 mg was used for each TL reading. All TL readings were carried out 24 h after irradiation, sufficient time to reach TL peak stability, except for the TL fading and emission spectrum measurements. Irradiations were done using a $^{60}Co$ γ-cell type source with an activity of 502.88 Ci and a dose rate of 0.64 kGy/h. EPR spectra were obtained utilizing an EPR spectrometer, model Miniscope 5000, operating in the X-band with a microwave frequency of 9.42 GHz. All spectra were obtained at room temperature (25 °C) using a mass of 150 mg of powdered sample placed inside a quartz capillary tube, which in turn was placed inside the EPR cavity. The recording parameters were: center field of 337 mT, modulation amplitude of 0.2 mT, modulation frequency of 100 kHz, and microwave power of 0.01 mW.

## 3. Results and discussion

### 3.1. X-ray diffraction (XRD) and X-ray fluorescence (XRF) studies

XRF analysis indicated that the dumortierite sample investigated here contained $SiO_2$ (68.5%), $Al_2O_3$ (26.3%), $P_2O_4$ (1.11%), $TiO_2$ (0.83%), $SO_3$ (0.31%), as well as other compounds at very low concentrations (Table 1). These compounds may play an important role in the TL and/or EPR properties of dumortierite.

Fig. 1 shows the diffractogram of the mineral acquired as dumortierite. Structural analysis of the XRD data using the QUALX program identified the presence of two crystalline phases: the dumortierite phase with 42% (ICDD PDF-2: No 01-084-1007), and the quartz phase (58%) (ICDD PDF-2: No 00-046-1045).

### 3.2. Thermoluminescence (TL) studies

Fig. 2 shows the glow curves of dumortierite previously annealed at 500, 600, 700, 800, 900, and 1200 °C for 1 h and irradiated with a γ-radiation dose of 2 kGy. The inset in Fig. 2 shows the natural TL of dumortierite as received. This sample shows three TL peaks: the first low-intensity peak at around 160 °C, the second at approximately 260 °C, and the third at 330 °C, which is the most intense and overlaps

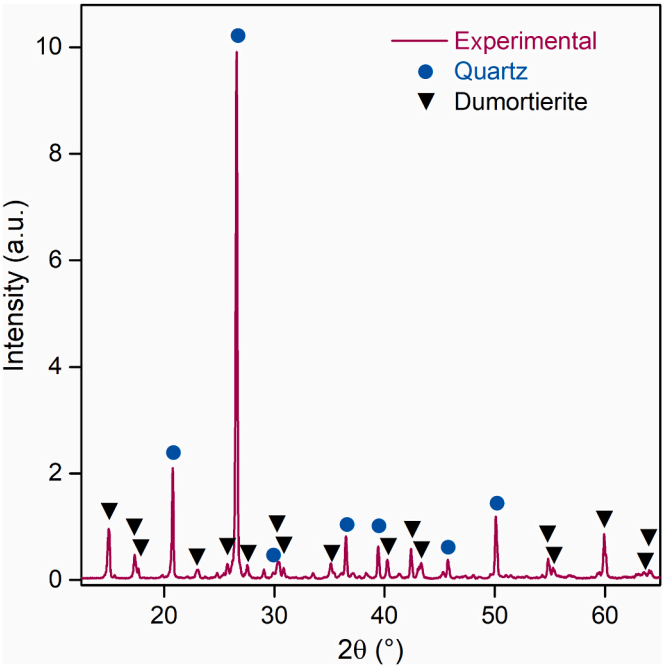


**Fig. 1.** XRD patterns of samples acquired as dumortierite. (●) belongs to quartz ($SiO_2$), and (▼) corresponds to dumortierite.

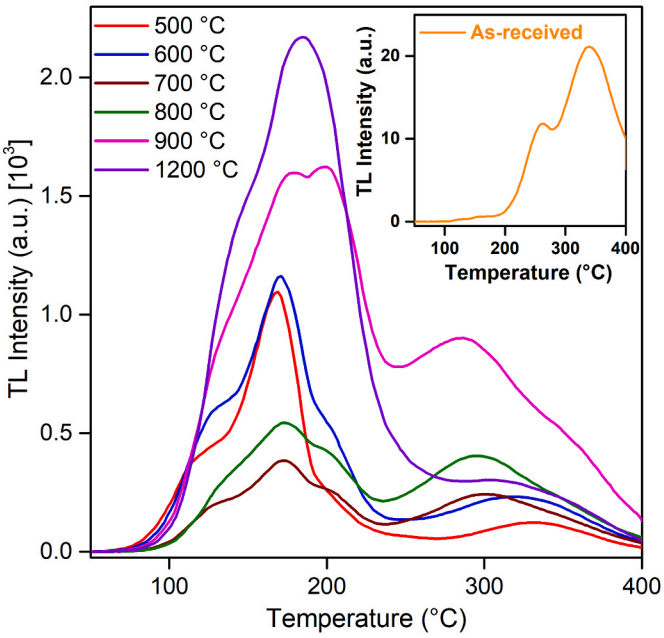


**Fig. 2.** TL glow curves of the dumortierite sample previously heat treated at 500, 600, 700, 800, 900, and 1200 °C for 2 h, and irradiated with a γ dose of 2 kGy from a $^{60}Co$ source before TL reading.

**Table 1**
Chemical composition of natural dumortierite determined by XRF analysis.

| Compound | $SiO_2$ | $Al_2O_3$ | $P_2O_5$ | $TiO_2$ | $K_2O$ | $Fe_2O_3$ | $SO_3$ | $As_2O_3$ | CaO | $Na_2O$ | SrO | $Cr_2O_3$ | $ZrO_2$ | ZnO |
|---|---|---|---|---|---|---|---|---|---|---|---|---|---|---|
| **(mass %)** | 68.5 | 26.3 | 1.11 | 0.83 | 0.45 | 0.36 | 0.31 | 0.28 | 0.23 | 0.08 | 0.06 | 0.02 | 0.02 | 0.01 |

with the peak at 260 °C. In Fig. 2, we observe that the glow curve varies in shape and intensity with heat treatment, which may be due to possible changes (creation and/or destruction) in the concentration of electron traps and/or recombination centers with annealing. For a heat treatment at 1200 °C, it can be observed that the TL intensity increases 65 times compared to the natural TL. Therefore, a heat treatment at 1200 °C was chosen for all further TL studies.

Fig. 3 shows the TL glow curves for all dumortierite samples previously heat-treated at 1200 °C and γ-irradiated with doses ranging from 5 Gy to 2 kGy. The results of this figure show in principle the presence of four superimposed peaks centered at 132, 200, 305, and 370 °C; the TL intensity of the peaks increases with dose, and their position remains unchanged. This result indicates that possibly most of the TL peaks are of first-order kinetics. The inset in Fig. 3 shows that for doses above 2 kGy, the high-temperature peaks (305 and 370 °C) overlap, forming a broad peak centered at approximately 350 °C. Due to the overlap between the TL peaks, it is necessary to perform a deconvolution study to analyze the behavior of each TL peak with dose.

Fig. 4 shows the behavior of the TL intensity of the peak at 200 °C as a function of γ-radiation dose. It is observed that the intensity of the peak at 200 °C presents a linear behavior up to a dose of 200 Gy, and then for doses higher than 200 Gy, it presents a supra-linear behavior, saturating for doses above 2 kGy.

The number of TL peaks contained in the glow curve and their kinetic parameters can be determined using two methods: Tm-Tstop [12] and deconvolution [13]. The Tm-Tstop method allows visualization of the number of TL peaks and gives information on the kinetic order of each TL peak. Fig. 5 displays the results of the Tm-Tstop method as outlined by McKeever [12]. These results indicate compatibility with at least six contributions associated with continuous electron trap distributions, with the exception of the first contribution, which is more closely aligned with a localized distribution, and additionally associated with general order kinetics (GOK) [13,14]. The invariance of the TL glow curve position to the dose in the dose-response exercise (Fig. 3) is linked to models related to the first-order kinetics (FOK) approach [13–15]. Alternatively, if not with FOK, it may align with the GOK approach, particularly when the order kinetics parameter "*b*" assumes low values.

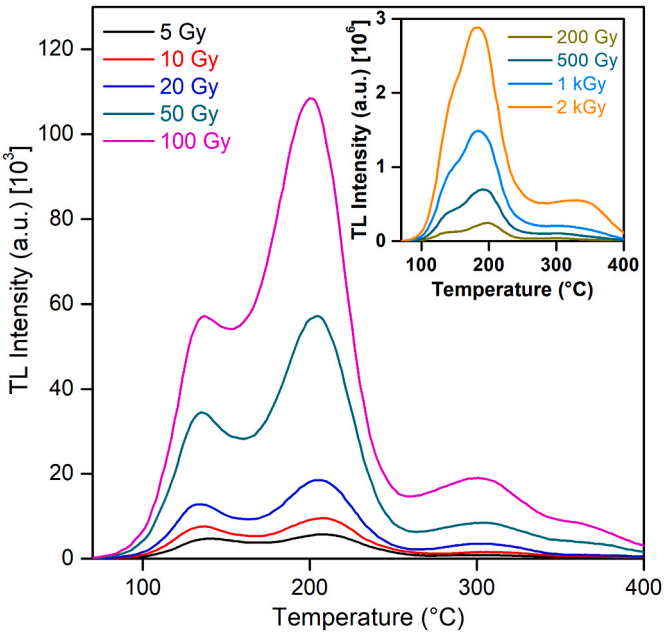


**Fig. 3.** TL glow curves of the dumortierite sample thermally treated at 1200 °C and then irradiated with γ doses between 5 Gy and 2 kGy. A heating rate of 4 °C/s was maintained, and a mass of approximately 4 mg was used for each measurement.

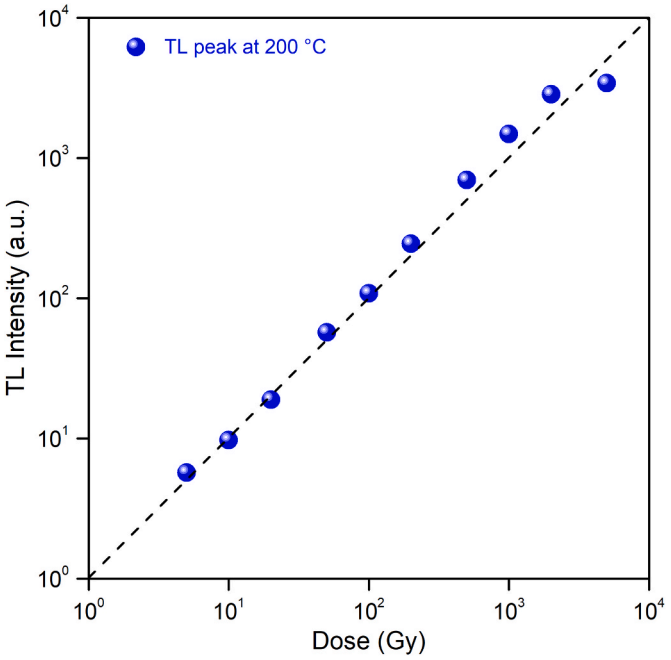


**Fig. 4.** The graph depicts the relationship between TL intensity and γ-radiation dose for the TL peak at 200 °C. The dashed lines (black) in the graph represent linearity.

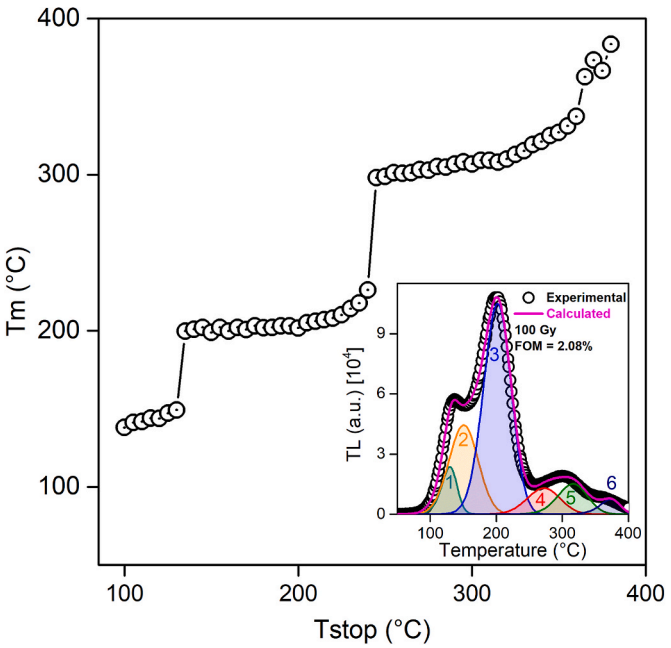


**Fig. 5.** Dependence of the maximum peak temperature (Tm) with the preheating temperature (Tstop) of the dumortierite sample. In inset: the deconvolution graph of the glow curve for the dumortierite samples thermally treated at 1200 °C and irradiated with a γ dose of 100 Gy. Six TL peaks were used with first-order kinetics (FOK) for each peak, except for peak 1 with general-order kinetics (GOK).

All of the glow curves in Fig. 3 were subjected to glow curve deconvolution through the use of the Computerized Glow Curve Deconvolution (CGCD) theoretical analysis approach, whose mathematical model used to fit experimental measurements is linked to Tm-Tstop results. The quality of these theoretical fits to experimental data is checked by the figure of merit (FOM) parameter [16]. The inset of

Fig. 5 depicts the outcome of the deconvolution analysis of the TL glow curves, showing a complex trapped electron structure derived from a linear combination of distributions associated with the FOK approach. This structure includes a trapped electron density $n(E)$ that correlates with both continuous and localized electron trap distributions. The deconvolution analysis performed in this work shows that the TL glow curves of dumortierite are composed of six peaks in the region between 100 °C and 400 °C.

The kinetic parameters, such as activation energy, maximum temperature, kinetic order, distribution width, and frequency factor, of the six TL peaks obtained by the deconvolution method for the glow curves of samples irradiated with γ-radiation from 5 to 2000 Gy are shown in Tables 2 and 3. For all glow curves, the FOM values are less than 3.25%, indicating that the deconvolution results are optimal. According to Ref. [16] the FOM parameter is acceptable when it is less than 5%.

The mathematical model utilized to perform the deconvolution fitting of the experimental curves is based on a linear combination of six functions, as shown in the following expression:

$$I_{TL}(T) = {}^{1}\mathrm{F}^{\mathrm{GOK}}_{\mathrm{localized}}\left(E_1, {}^{1}T_{\mathrm{Max}}, {}^{1}I_{\mathrm{Max}}, b; T\right) + \sum_{i=2,3,4,5,6} {}^{i}\mathrm{F}^{\mathrm{FOK}}_{\mathrm{continuous}}\left(E_i, {}^{i}T_{\mathrm{Max}}, {}^{i}I_{\mathrm{Max}}, \sigma; T\right) \quad (1)$$

Gaussian distribution was used for the trapped electron density $n(E)$ [13], when assuming analytical functions related to continuous trap distributions, as follows:

$$n(E) = \frac{n_0}{\sqrt{2\pi\sigma^2}} e^{-\frac{(E-E_0)}{2\sigma^2}} \quad (2)$$

Fig. 6 shows the emission spectrum of the dumortierite sample after irradiation with a dose of 80 Gy. This dose was necessary due to the presence of the monochromator located in front of the photomultiplier tube. Analyzing the spectrum of the dumortierite sample, we can identify a main emission that is centered at 350 nm, corresponding to the TL peaks at 90, 120, and 200 °C. There are also lower emissions at 475 nm and 580 nm. The emission at 475 nm contributes to the 90 °C TL peak, and the emission at 580 nm contributes to the 200 °C peak. The presence of the low temperature peak around 90 °C is due to the fact that the TL reading to obtain the TL spectrum was taken immediately.

A good TL dosimeter should have a constant TL response at room temperature for a large period after absorbing the radiation energy, i.e., have a minimum fading (reduction of the TL response at room temperature) up to the TL reading. The fading is related to the ease of electron release from unstable traps at room temperature. For this reason, a TL response fading study was performed for the dumortierite sample previously heat treated at 1200 °C, and irradiated with a dose of 80 Gy, and stored in a dark room at room temperature for different times. Fig. 7 shows the peak fading plot at 132, 200, 305, and 370 °C using the maximum TL intensity. We can observe that the peak intensity at 132 and 200 °C shows a decay of 7% and 2%, respectively, in the first 3 h, and then both peaks remain unchanged with storage time up to a 30-day test. On the other hand, the TL glow peaks at 305 and 370° present a low intensity response. However, both peaks present good stability with storage time. The good TL response and the stability of the luminescent signal corresponding to the TL peak at 200 °C indicate that this material is promising for dosimetry.

### 3.3. Electron paramagnetic resonance (EPR) studies

The effect of heat treatment on the EPR spectrum of the natural dumortierite sample before irradiation was also investigated. For this study, the powdered natural dumortierite sample was heat treated at 500, 600, 700, 800, 900, and 1200 °C for an interval of 1 h. Fig. 8 shows the EPR spectra for each heat treatment, irradiated with a γ-radiation dose of 1 kGy. It is observed that the EPR intensity of the signals around $g = 2.001$ increases with the treatment temperature, being the most intense for a 1200 °C heat treatment. A similar result presents the TL response of this material with the same heat treatment, evidencing a possible correlation between defect centers responsible for the TL response and the EPR spectrum. The room-temperature EPR spectrum of the γ-irradiated dumortierite sample with heat treatment at 1200 °C is shown in Fig. 8 (γ-dose: 1 kGy). The spectrum exhibits a distinct shape indicative of a defect center displaying an axially symmetric $g$-tensor while lacking hyperfine splitting. Thermal annealing experiments reveal the presence of a single center, denoted as center I, in γ-irradiated dumortierite mineral. The specific assignment of this center will be addressed in subsequent discussions. The principal $g$-values of the center are determined to be $g_{\parallel} = 2.0009$ and $g_{\perp} = 2.0017$ and the linewidth is about 1 Gauss.

To study the effect of radiation exposure on the EPR spectrum, the dumortierite sample, previously heat-treated at 1200 °C, was irradiated with γ-rays in the dose range of 5 Gy and 2 kGy. Fig. 9 shows that the EPR peak-peak intensity of center I increases with the irradiation dose. The inset of Fig. 9 shows the EPR response of center I as a function of γ-radiation dose between 5 Gy and 2 kGy. Analyzing the dose-response curve with logarithmic axes in the same scale, it can be observed that the EPR response has a linear behavior in the dose range from 5 Gy to 100 G, then a sub-linear behavior up to 1 kGy, and for doses above this value it saturates.

XRD analysis has shown that the dominant component of the mineral is quartz. Several defect centers can form in an oxide system like quartz upon γ-irradiation. These are the well-known E′-center, Ge center, peroxy radical, Al center, and Ti center. Some of these centers, like the Al center and the Ti center, are observable at low temperatures due to their short spin-lattice relaxation times. On the other hand, the E′-center, the Ge center, and the peroxy radical are seen at room temperature. A number of studies have been carried out on the E′-center, and the center displays an axial $g$-tensor with principal values of $g_{\parallel} = 2.0018$ and $g_{\perp} = 2.0005$ [17]. The Ge center is characterized by the $g$-values 1.9959,

**Table 2**
Details of activation energy ($E$), maximum temperature (T), kinetics order ($b$), distribution width ($\sigma$), and frequency factors ($s$) of the TL peaks 1, 2, 3 of the dumortierite crystal obtained by the deconvolution method of the glow curves for different doses. Bottom: the average.

| Dose (Gy) | FOM (%) | Peak 1: GOK (Localized) | | | | Peak 2: FOK (Continuous) | | | | Peak 3: FOK (Continuous) | | | |
|---|---|---|---|---|---|---|---|---|---|---|---|---|---|
| | | $E$ (eV) | T (°C) | $b$ | $s$ ($s^{-1}$) | $E$ (eV) | T (°C) | $\sigma$ (eV) | $s$ ($s^{-1}$) | $E$ (eV) | T (°C) | $\sigma$ (eV) | $s$ ($s^{-1}$) |
| 5 | 2.76 | 1.3885 | 134.54 | 1.3962 | $5.66{\cdot}10^{16}$ | 1.71119 | 162.46 | 0.079778 | $2.63{\cdot}10^{19}$ | 1.8598 | 198.71 | 0.071392 | $2.84{\cdot}10^{19}$ |
| 10 | 3.25 | 1.4037 | 135.40 | 1.3742 | $8.07{\cdot}10^{16}$ | 1.70476 | 164.26 | 0.080194 | $1.81{\cdot}10^{19}$ | 1.8742 | 199.47 | 0.070595 | $3.77{\cdot}10^{19}$ |
| 20 | 2.73 | 1.4065 | 134.32 | 1.3715 | $9.80{\cdot}10^{16}$ | 1.70516 | 162.06 | 0.080175 | $2.33{\cdot}10^{19}$ | 1.8747 | 201.48 | 0.070568 | $3.11{\cdot}10^{19}$ |
| 50 | 1.85 | 1.4075 | 131.31 | 1.3654 | $1.38{\cdot}10^{17}$ | 1.70089 | 158.32 | 0.080452 | $3.12{\cdot}10^{19}$ | 1.8780 | 203.70 | 0.070401 | $2.70{\cdot}10^{19}$ |
| 100 | 2.08 | 1.4136 | 129.74 | 1.3600 | $1.95{\cdot}10^{17}$ | 1.70283 | 155.09 | 0.080330 | $4.73{\cdot}10^{19}$ | 1.8790 | 206.14 | 0.070339 | $2.18{\cdot}10^{19}$ |
| 200 | 2.36 | 1.4136 | 133.91 | 1.4100 | $1.26{\cdot}10^{17}$ | 1.70283 | 153.80 | 0.080330 | $5.47{\cdot}10^{19}$ | 1.8790 | 208.40 | 0.070339 | $1.74{\cdot}10^{19}$ |
| 500 | 1.64 | 1.4123 | 130.58 | 1.3631 | $1.71{\cdot}10^{17}$ | 1.70222 | 152.32 | 0.080364 | $6.35{\cdot}10^{19}$ | 1.8779 | 210.02 | 0.070401 | $1.44{\cdot}10^{19}$ |
| 1000 | 3.24 | 1.4013 | 130.90 | 1.3799 | $1.20{\cdot}10^{17}$ | 1.70501 | 152.72 | 0.080151 | $6.56{\cdot}10^{19}$ | 1.8773 | 210.80 | 0.070431 | $1.32{\cdot}10^{19}$ |
| 2000 | 2.39 | 1.4057 | 132.83 | 1.3709 | $1.12{\cdot}10^{16}$ | 1.70216 | 156.19 | 0.080370 | $4.10{\cdot}10^{19}$ | 1.8755 | 212.89 | 0.070527 | $1.03{\cdot}10^{19}$ |
| **Average** | | | | | | 1.7041 (4) | 157.5 (6) | 0.08024 (3) | $4.12(2){\cdot}10^{19}$ | 1.875 (1) | 205.7 (6) | 0.07056 (4) | $2.3(1){\cdot}10^{19}$ |

**Table 3**
Details of activation energy ($E$), maximum temperature (T), order of kinetics ($b$), distribution width ($\sigma$), and frequency factors ($s$) of the TL peaks 4, 5, and 6 of the dumortierite crystal obtained by the deconvolution method of the glow curves for different doses. Bottom: the average.

| Dose (Gy) | FOM (%) | Peak 4: FOK (Continuous) | | | | Peak 5: FOK (Continuous) | | | | Peak 6: FOK (Continuous) | | | |
|---|---|---|---|---|---|---|---|---|---|---|---|---|---|
| | | $E$ (eV) | T (°C) | $\sigma$ (eV) | $s$ ($s^{-1}$) | $E$ (eV) | T (°C) | $\sigma$ (eV) | $s$ ($s^{-1}$) | $E$ (eV) | T (°C) | $\sigma$ (eV) | $s$ ($s^{-1}$) |
| 5 | 2.76 | 1.9546 | 254.9 | 0.08120 | $1.47{\cdot}10^{18}$ | 2.1612 | 322.37 | 0.07070 | $5.52{\cdot}10^{17}$ | 2.6225 | 369.1 | 0.04714 | $1.12{\cdot}10^{20}$ |
| 10 | 3.25 | 1.9953 | 256.7 | 0.07873 | $3.13{\cdot}10^{18}$ | 2.2269 | 321.46 | 0.06745 | $2.19{\cdot}10^{18}$ | 2.7986 | 369.3 | 0.03910 | $2.84{\cdot}10^{21}$ |
| 20 | 2.73 | 1.9941 | 265.1 | 0.07879 | $1.50{\cdot}10^{18}$ | 2.2344 | 321.74 | 0.06708 | $2.49{\cdot}10^{18}$ | 2.7995 | 369.8 | 0.03896 | $2.77{\cdot}10^{21}$ |
| 50 | 1.85 | 1.9914 | 271.2 | 0.07893 | $8.55{\cdot}10^{17}$ | 2.2295 | 320.95 | 0.06737 | $2.40{\cdot}10^{18}$ | 2.7568 | 371.6 | 0.04091 | $1.09{\cdot}10^{21}$ |
| 100 | 2.08 | 2.0075 | 277.5 | 0.07802 | $7.24{\cdot}10^{17}$ | 2.2435 | 320.92 | 0.06662 | $3.18{\cdot}10^{18}$ | 2.8511 | 375.4 | 0.03678 | $4.50{\cdot}10^{21}$ |
| 200 | 2.36 | 2.0075 | 281.3 | 0.07802 | $5.38{\cdot}10^{17}$ | 2.2435 | 332.73 | 0.06662 | $1.30{\cdot}10^{18}$ | 2.8511 | 382.4 | 0.03678 | $2.55{\cdot}10^{21}$ |
| 500 | 1.64 | 2.0038 | 280.8 | 0.07814 | $5.17{\cdot}10^{17}$ | 2.2501 | 318.68 | 0.06638 | $4.32{\cdot}10^{18}$ | 2.7597 | 382.4 | 0.04126 | $4.90{\cdot}10^{20}$ |
| 1000 | 3.24 | 2.0110 | 271.3 | 0.07793 | $1.30{\cdot}10^{18}$ | 2.2410 | 320.80 | 0.06677 | $3.05{\cdot}10^{18}$ | 2.7402 | 378.7 | 0.04154 | $4.59{\cdot}10^{20}$ |
| 2000 | 2.39 | 1.9940 | 262.8 | 0.07886 | $1.82{\cdot}10^{18}$ | 2.2127 | 320.30 | 0.06829 | $1.80{\cdot}10^{18}$ | 2.6881 | 381.5 | 0.04310 | $1.44{\cdot}10^{20}$ |
| **Average** | | 1.995 (2) | 269 (1) | 0.0787 (1) | $1.2(1){\cdot}10^{18}$ | 2.227 (3) | 322(1) | 0.0675 (2) | $2.4(1){\cdot}10^{18}$ | 2.763 (9) | 376 (1) | 0.0406 (4) | $1.85(2){\cdot}10^{21}$ |

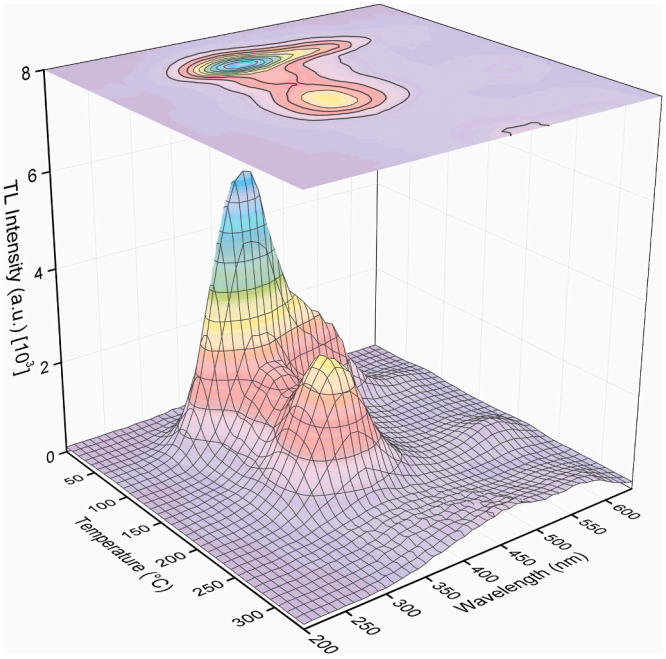


**Fig. 6.** 3D representation (bottom) and contour plot (top) of the TL spectrum of the dumortierite sample previously treated at 1200 °C and irradiated with a dose of 80 Gy.

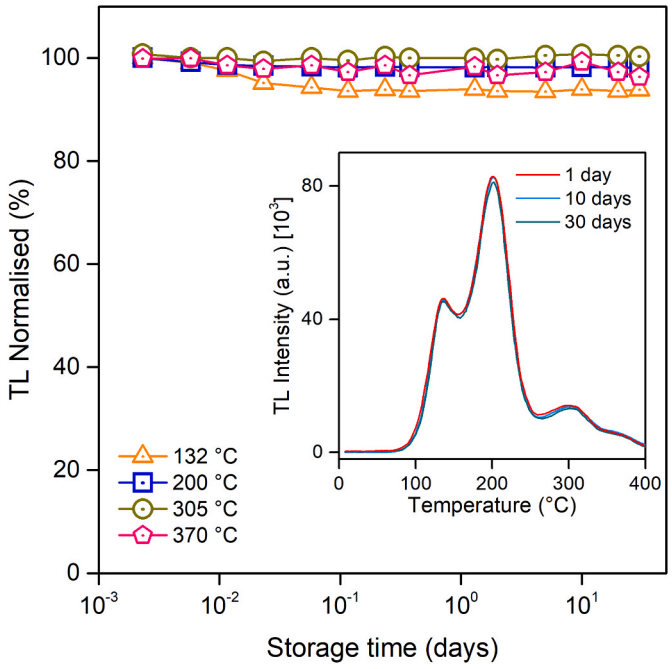


**Fig. 7.** Normalized TL fading of peaks at 132 and 200 °C as a function of storage time interval.

1.9970, and 2.0005 [18]. Peroxy radical also displays a rhombic $g$-tensor, like Ge center, with principal values of 2.0014, 2.0074, and 2.067 [19].

Apart from these centers, $F^+$ center (an electron trapped at an anion vacancy) may also be formed induced by γ-irradiation. In its first observation in an alkali halide system, a large linewidth of about 100 Gauss was observed for the center [20]. The inherent linewidth, however, is about 1 Gauss as observed in MgO [21]. The width of the line varies across different systems, depending on the degree of electron delocalization and its interaction with the nearest cations situated one bond length away from the anion vacancy. The neighboring ions may also include ions in the successive shells. Further, the magnetic moments and the relative abundance of the isotopes of the neighboring ions are also important factors that contribute to the linewidth displayed by the center. Large linewidths are exhibited by the center in alkali halides as there is considerable delocalization of the unpaired spin. The unpaired electron in these systems interacts not only with the immediate neighbors but also with alkali and halide ions in successive neighboring shells. Examples of alkali halides where large linewidths are observed are KCl (20 Gauss) and LiCl (56 Gauss) [22]. In BaO [23], a linewidth of 3.5 Gauss is observed. In addition to alkali halides, an electron trapped at an anion vacancy (i.e., $F^+$ center) has been observed in oxide systems. In general, $F^+$ center displays a $g$-value that is isotropic and close to the free-electron value of 2.0023. However, the $g$-shift can be positive or negative. In the present mineral system, the $g$-shifts are negative and the linewidth is not large. These observations allow a tentative assignment of the center to an $F^+$ center. Fig. 10 displays the thermal annealing behavior of the center. It is observed that the center becomes unstable at about 95 °C and the intensity begins to decrease and the center decays in the temperature range 95 °C – 225 °C. It thus appears that center I could be associated with the TL peak at 200 °C.

It may be mentioned that the observed $g$-values appear to be similar to the ones exhibited by the E′-center. However, $g_{\|} > g_{\perp}$ for the E′-center and the defect center in the present mineral exhibits $g$-values where $g_{\|} < g_{\perp}$. Further, it is well known that the E′-center ESR signal saturates at very low microwave powers (at about 0.1 mW). Fig. 11 displays the microwave power saturation behavior of the E′-center [24]. A microwave power saturation experiment has been carried out for the center observed in the present system and the results are presented in the inset of Fig. 11. It is seen that the signal saturates at about 1.0 mW. These observations and the observed $g$-values exclude the assignment of the

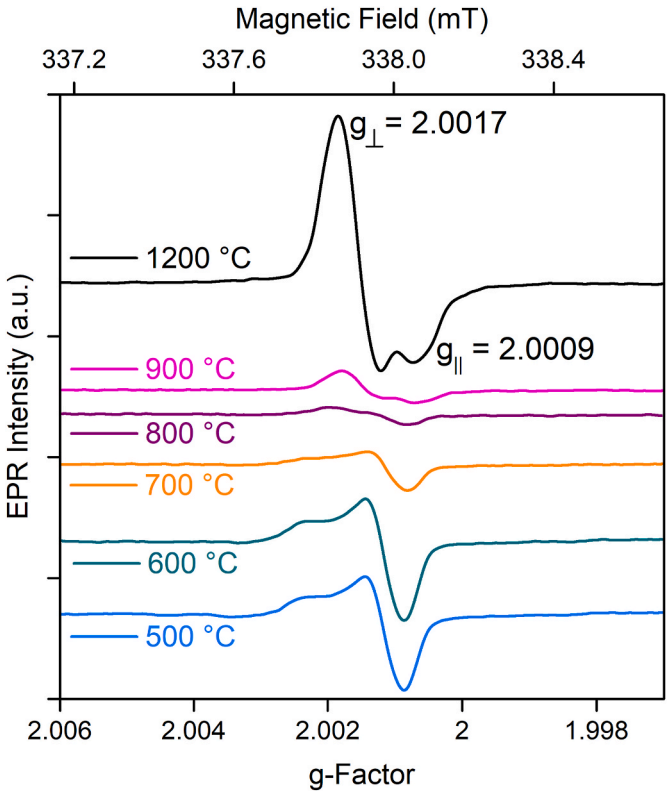


**Fig. 8.** Room temperature EPR spectrum of the dumortierite sample with heat treated at 500, 600, 700, 800, 900, and 1200 °C for 2 h and irradiated with a 1 kGy γ dose from a $^{60}$Co source before the EPR measurement.

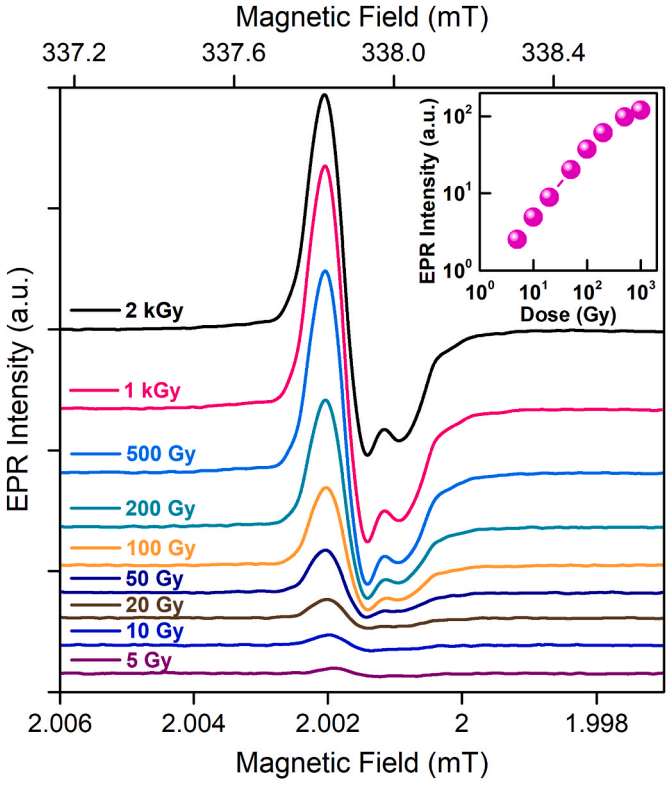


**Fig. 9.** EPR spectra of the dumortierite samples heat treated at 1200 °C and irradiated at different doses between 5 Gy and 2 kGy. The inset shows the behavior of the EPR intensity as a function of the γ-dose radiation.

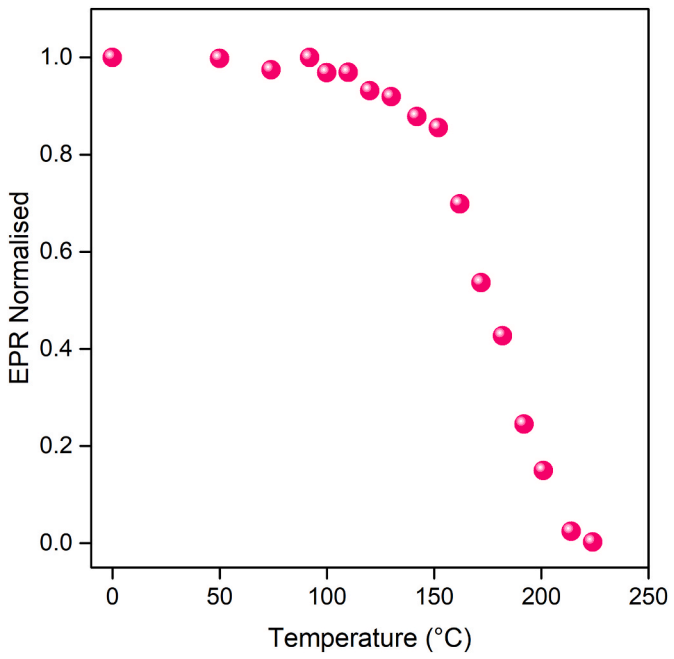


**Fig. 10.** Thermal annealing behavior of center I in the dumortierite sample.

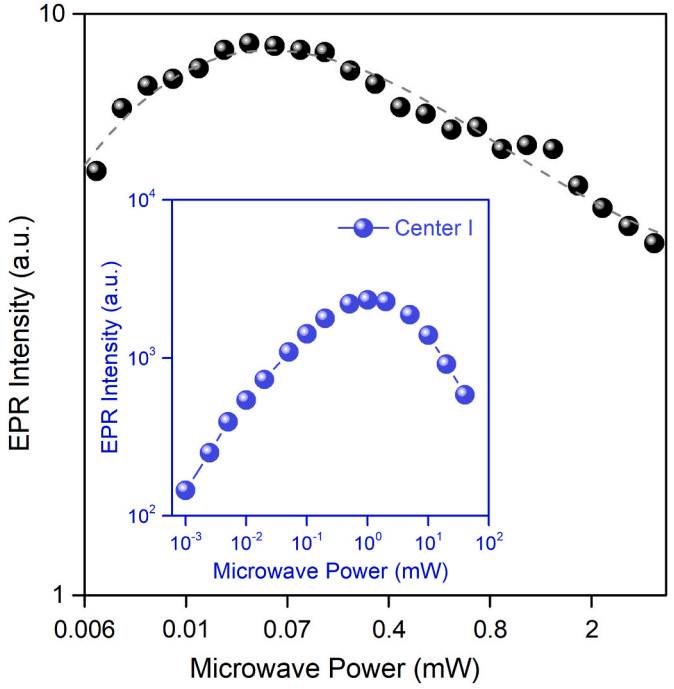


**Fig. 11.** Microwave power saturation behavior of the E′-center (adapted from Benny et al. [23]). In inset, microwave power saturation plot of the center in the irradiated dumortierite sample.

observed center in dumortierite to an E′-center.

It is observed that center I displays an axially symmetric *g*-tensor. $F^+$ centers characterized by an axially symmetric *g*-tensor have been observed in Yttria stabilized Zirconia (YSZ; $ZrO_2$: Y) [25], and $CaZrO_3$: Tb [26]. The *g*-shifts are negative in these systems. In general, $F^+$ centers exhibit isotropic *g*-values. The axial nature of the *g*-tensor in YSZ was interpreted by invoking the presence of a symmetry-breaking defect center at an anion site close to the $F^+$ center that explains the axial nature of the *g*-tensor. A neutral F center (an oxygen vacancy with two

electrons) was considered that has a probability of forming in the YSZ lattice due to the presence of oxygen vacancies. In quartz lattice, oxygen vacancies will be present and γ-irradiation can induce F center formation close to the center I. It may be mentioned that an $F^+$ center with axially symmetric *g*-tensor along with positive *g*-shifts has been observed in X-irradiated Sodium β-alumina ($g_{\parallel} = 2.0076$ and $g_{\perp} = 2.0032$) [27].

## 4. Conclusions

The investigation of the crystal structure and chemical composition by XRD and XRF, respectively, showed the presence of dumortierite and quartz crystals in the sample acquired as dumortierite. The shape and intensity of the TL glow curve of dumortierite show high dependence on the heat treatment temperature. For a heat treatment temperature of 1200 °C for 1 h, it shows the highest sensitization in its TL response. The dumortierite sample with heat treatment at 1200 °C shows six TL peaks in the region of 100 – 400 °C; these peaks have low fading. Moreover, the peaks around 200 °C show a linear behavior with γ-radiation dose. A single defect center has been observed in the γ-irradiated mineral dumortierite, and the center is tentatively identified as an $F^+$ center. The center correlates with the TL peak at 132 °C and 200 °C.

## CRediT authorship contribution statement

**Betzabel N. Silva-Carrera:** Methodology, Formal analysis, Data curation, Investigation, Visualization. **T.K. Gundu Rao:** Writing – original draft, Validation, Supervision, Methodology, Formal analysis, Investigation, Writing – review & editing. **Betzabeth J. Lopez-Flores:** Investigation, Methodology. **Jorge S. Ayala-Arenas:** Investigation, Funding acquisition. **René R. Rocca:** Investigation, Methodology. **J.F. Benavente:** Validation, Software, Investigation, Formal analysis, Writing – original draft, Writing – review & editing. **Jose F.D. Chubaci:** Investigation, Methodology. **Nilo F. Cano:** Writing – original draft, Formal analysis, Conceptualization, Data curation, Funding acquisition, Supervision, Validation, Writing – review & editing.

## Declaration of competing interest

The authors declare that they have no known competing financial interests or personal relationships that could have appeared to influence the work reported in this paper.

## Data availability

Data will be made available on request.

## Acknowledgment

This work was supported by CONCYTEC-PROCIENCIA, Peru, in the framework of the call E041-2021-02 (Process number 047-2021-FONDECYT). In addition, the authors wish to thank Ms. E. Somessari from the Institute for Energy and Nuclear Researches (IPEN), Brazil, for kindly carrying out the irradiation of the samples.

## References

[1] N.F. Cano, T.K. Gundu Rao, J.S. Ayala-Arenas, C.D. Gonzales-Lorenzo, L. M. Oliveira, S. Watanabe, TL in green tourmaline: study of the centers responsible for the TL emission by EPR analysis, J. Lumin. 205 (2019) 324–328, https://doi.org/10.1016/j.jlumin.2018.09.034.

[2] T.K. Gundu Rao, N.F. Cano, B.N. Silva-Carrera, R.M. Ferreira, H.S. Javier-Ccallata, S. Watanabe, Centers responsible for the TL peaks of willemite mineral estimated by EPR analysis, J. Lumin. 177 (2016) 139–144, https://doi.org/10.1016/j.jlumin.2016.04.026.

[3] N.F. Cano, A.R. Blak, J.S. Ayala-Arenas, S. Watanabe, Mechanisms of TL for production of the 230 °C peak in natural sodalite, J. Lumin. 131 (2011) 165–168, https://doi.org/10.1016/j.jlumin.2010.09.027.

[4] A. Pieczka, R.J. Evans, E.S. Grew, L.A. Groat, C. Ma, G.R. Rossman, The dumortierite supergroup. I. a new nomenclature for the dumortierite and holtite groups, Mineral. Magazine 77 (2013) 2825–2839, https://doi.org/10.1180/minmag.2013.077.6.09.

[5] A.H. Horn, Y. Fuchs, S.C. Neves, E. Balan, J. Linarè, The occurrence of dumortierite in the Espinhaço Range, Minas Gerais, Brazil, and its mineralogical crystallographic comparison with other specimen, Revista Espinhaço 3 (2014) 4–14.

[6] G. Werding, W. Schreyer, Synthetic dumortierite: its PTX-dependent compositional variations in the system $Al_2O_3$-$B_2O_3$-$SiO_2$-$H_2O$, Contr. Mineral. Petrol. 105 (1990) 11–24, https://doi.org/10.1007/BF00320963.

[7] A.N. Platonov, K. Langer, C. Chopin, M. Andrut, M.N. Taran, $Fe^{2+}$-$Ti^{4+}$ charge-transfer in dumortierite, Eur. J. Mineral 12 (2000) 521–528, https://doi.org/10.1127/0935-1221/2000/0012-0521.

[8] L.V. Ranaweera, L.R.K. Perera, Y. Hiroi, Blue dumortierite from, Habarana, Sri Lanka: field occurrence and mineral chemistry, J. Geol. Soc. Sri Lanka 12 (2007) 53–74.

[9] E.S. Grew, Borosilicates (exclusive of tourmaline) and boron in rock-forming minerals in metamorphic environments, Rev. Mineral. Geochem. 33 (1996) 387–502.

[10] R. R, Meshram, K.B. Ingle, Mineralogy and origin of dumortierite from Girola area, Bhandara district, Eastern Maharashtra, J. Geol. Soc. India 79 (2012) 181–188, https://doi.org/10.1007/s12594-012-0020-4.

[11] C.O. Choo, J.J. Kim, Mineralogical studies of dumortierite from the Miryang clay deposit, Korea, Geosci. J. 5 (2001) 273–279, https://doi.org/10.1007/BF02912697.

[12] S.W.S. McKeever, Thermoluminescence in Solids, Cambridge University Press, Cambridge, 1985.

[13] J.F. Benavente, J.M. Gómez-Ros, A.M. Romero, Thermoluminescence glow curve deconvolution for discrete and continuous trap distributions, Appl. Radiat. Isotopes 153 (2019) 108843, https://doi.org/10.1016/j.apradiso.2019.108843.

[14] R. Chen, S.W.S. McKeever, Theory of Thermoluminescence and Related Phenomena, World Scientific, 1997, pp. 110–117.

[15] A.J.J. Bos, Theory of thermoluminescence, Radiat. Meas. 41 (2006) S45–S56, https://doi.org/10.1016/j.radmeas.2007.01.003.

[16] H.G. Balian, N.W. Eddy, Figure of merit (FOM), an improved criterion over the normalized chi-squared test for assessing goodness of fit of gamma-ray spectral peaks, Nucl. Instrum. Methods 145 (1977) 389–395, https://doi.org/10.1016/0029-554X(77)90437-2.

[17] S. Toyoda, H.P. Schwarcz, Counterfeit $E_1'$ signal in quartz, Radiat. Meas. 27 (1997) 59–66, https://doi.org/10.1016/S1350-4487(96)00073-X.

[18] J.H. Mackey, EPR study of impurity-related color centers in germanium-doped quartz, J. Chem. Phys. 39 (1963) 74–83, https://doi.org/10.1063/1.1734035.

[19] E.J. Friebele, D.L. Griscom, M. Stapelbroek, R.A. Weeks, Fundamental defect centers in glass: the peroxy radical in irradiated, high-purity, fused silica, Phys. Rev. Lett. 42 (1979) 1346, https://doi.org/10.1103/PhysRevLett.42.1346.

[20] C.A. Hutchison, Paramagnetic resonance absorption in crystals colored by irradiation, Phys. Rev. 75 (1949) 1769–1770, https://doi.org/10.1103/PhysRev.75.1769.2.

[21] J.E. Wertz, P. Auzins, R.A. Weeks, R.H. Silsbee, Centers in magnesium oxide; confirmation of the spin of magnesium-25, Phys. Rev. 107 (1957) 1535–1537, https://doi.org/10.1103/PhysRev.107.1535.

[22] W.C. Holton, H. Blum, Paramagnetic resonance of F centers in alkali halide, Phys. Rev. 125 (1962) 89–103, https://doi.org/10.1103/PhysRev.125.89.

[23] A.J. Tench, R.L. Nelson, Electron spin resonance of F centres in irradiated $^{43}$CaO and other alkaline earth oxides, Proc. Phys. Soc. 92 (1967) 1055, https://doi.org/10.1088/0370-1328/92/4/328.

[24] P.G. Benny, M.R. Shah, S. Sabharwal, B.C. Bhatt, T.K. Gundu Rao, Dosimetric Characterization and Identification of TL Defect Centres in Sand for its Application in Sludge Irradiators as an in Situ Dosimeter, BARC Report, 2003. BARC/2003/E/024.

[25] J.M. Costantini, F. Beuneu, D. Gourier, C. Trautmann, G. Calas, M. Toulemonde, Colour centre production in yttria-stabilized zirconia by swift charged particle irradiations, J. Phys. Condens. Matter 16 (2004) 3957, https://doi.org/10.1088/0953-8984/16/23/014.

[26] V. Singh, S. Watanabe, T.K. Gundu Rao, K. Al-Shamery, M. Haase, Y.D. Jho, Synthesis, characterisation, luminescence and defect centres in solution combustion synthesised CaZrO3:Tb3+ phosphor, J. Lumin. 132 (2012) 2036–2042, https://doi.org/10.1016/j.jlumin.2012.03.027.

[27] K. O'Donnell, R.C. Barklie, B. Henderson, EPR and optical absorption studies of radiation-produced defects in sodium beta -alumina, J. Phys. C Solid State Phys. 11 (1978) 3871, https://doi.org/10.1088/0022-3719/11/18/022.